Model Identification and FE Simulations:
Effect of Different Yield Loci and Hardening Laws
in Sheet Forming

P. Flores*, L. Duchêne♣, T. Lelotte*, C. Bouffioux*, F. El Houdaigui*,
A. Van Bael**, S. He**, J. Duflou&, A.M.Habraken*

*Dept of Mechanics of Solids and Materials, Univ. de Liège, Chemin des Chevreuils 1, B-4000 Liege, Belgium
♣COBO Department, Royal Military Academy, Renaissancelaan 30, B-1000 Brussel Belgium;
**Department MTM, Katholieke Universiteit Leuven, Kasteelpark Arenberg 44, B-3001 Leuven, Belgium
&Department PMA, Katholieke Universiteit Leuven, Celestijnlaan 300B, B3001 Leuven, Belgium

Abstract. The bi-axial experimental equipment [1] developed by Flores enables to perform Baushinger shear tests and successive or simultaneous simple shear tests and plane-strain tests. Such experiments and classical tensile tests investigate the material behavior in order to identify the yield locus and the hardening models. With tests performed on two steel grades, the methods applied to identify classical yield surfaces such as Hill or Hosford ones as well as isotropic Swift type hardening or kinematic Armstrong–Frederick hardening models are explained. Comparison with the Taylor-Bishop-Hill yield locus is also provided. The effect of both yield locus and hardening model choice will be presented for two applications: Single Point Incremental Forming (SPIF) and a cup deep drawing.

INTRODUCTION

In practice, different metal forming processes such as deep drawing, stamping or bending are required to manufacture automotive parts, beverage or food cans, steel sheet panels used in aeronautics or civil engineering applications. Computer models try to replace the expensive and time-consuming trial-and-error methods used in conventional design. The Finite Element Method (FEM) is quite successful to simulate metal forming processes, but accuracy depends both on the constitutive laws used and their material parameters identification.

For instance, the final shape of a product is strongly linked to the plastic material flow and to the springback phenomenon. Plastic anisotropy explains the undulated rims called ears, which appear in a cup produced by cylindrical tools applied on a circular blank. The classical isotropic elasto-plastic von Mises law predicts no rim at all. The simple quadratic anisotropic elasto-plastic Hill law often simulates an inaccurate four-earing profile. More complex models relying on crystal plasticity and a homogenization approach provide results that are closer to the experimental observations, but they are quite greedy from a CPU time point of view.

This paper uses both simple classical phenomenological laws and micro-macro constitutive models based on crystal plasticity. Classical phenomenological models roughly consist of fitting of functions on experimental results. They provide only crude tools the quality of which depends both on the complexity of the chosen functions and on the type of experiments used to identify them.

The bi-axial experimental equipment [1] developed by Flores enables to perform successive or simultaneous simple shear tests and plane-strain tests. Such experiments applied on samples cut in different directions from the rolling direction investigate the plasticity entrance and identify the initial yield locus. Stress contours at identical plastic work can also be drawn. The next section shows the difference between experimental points and yield loci defined by a phenomenological model or deduced from texture measurement and crystal plasticity.

Kinematic hardening models are identified by cyclic shear tests showing the Baushinger effect. Orthogonal tests are performed by successive simple shear and tensile tests. Such experimental results provide the necessary data to support simple models, like the one suggested by Armstrong–Frederick [2]

one or more complex ones like the Teodosiu model [3].

After the presentation of the method used to identify the yield locus and the hardening behavior for two materials, two applications where the simulation results strongly depend on the model choice and identification are described: the Single Point Incremental Forming (SPIF) process and the deep drawing process.

MODEL IDENTIFICATION

The first step is the identification of the initial yield locus shape. The case of DC06 IF steel sheet of 0.8 mm is presented as this material shows a quite strong anisotropy. The second step is the hardening behavior. The DP1000 dual phase sheet (1.6 mm thick) is studied and this example confirms that both steps cannot be completely decoupled. Tensile tests were performed in a standard tensile test machine of 20 kN capacity (with a normalized specimen) while the plane-strain and simple shear tests were performed in the bi-axial machine developed at the University of Liège [1].

Yield Locus Shape

First, the texture was measured by X-Ray diffraction and a set of 2000 representative crystal orientations was chosen [4]. The yield locus shape has been computed by a crystal plastic approach (Taylor-Bishop-Hill model). Then, tensile, plane-strain and simple shear tests were performed at 0°, 45° and 90° from the sheet rolling direction (RD). The results of two different methods used to identify the Hill 1948 and the Hosford 1979 yield criteria are compared hereafter.

Equation (1) defines the Hill 1948 yield criterion in plane stress state with the material parameters H, G, F, N and the initial yield stress σ_0 for a tensile test in the RD.

$$\Phi_{Hill}\left(\underline{\sigma}\right) = \frac{1}{2}\left[(H+G)\sigma_{xx}^2 + (H+F)\sigma_{yy}^2 - 2H\sigma_{xx}\sigma_{yy} + 2N\sigma_{xy}\right] = \sigma_0^2 \quad (1)$$

Unlike the Hill yield criterion, the Hosford 1979 one is non-quadratic. The main advantage is that the fitting of the value of the exponent ensures a good approximation of the experimental data [5]. Recommended values are a=6 for bcc materials and

a=8 for fcc materials [6]. The main drawback of this criterion is the lack of shear stresses, as shown by equation (2) in plane stress.

$$\Phi_{Hosford}\left(\underline{\sigma}\right) = H\left|\sigma_{xx} - \sigma_{yy}\right|^a + G\left|\sigma_{xx}\right|^a + F\left|\sigma_{yy}\right|^a = \sigma_0^a \quad (2)$$

The first identification method only uses the Lankford coefficients $r_{0°}$, $r_{45°}$, $r_{90°}$ (i.e; the ratio between the transversal plastic strain rate and the thickness plastic strain rate) measured during tensile tests at 0°, 45° and 90° from the RD. Extensometers measure axial and transversal strains. The thickness strain is computed by volume conservation. Using associated plasticity theory, the flow rule defines the plastic strain rate proportional to the stress derivative of the yield locus, $\underline{\dot{\varepsilon}}^p = \dot{\lambda} \cdot \partial \underline{\Phi} / \partial \underline{\sigma}$. The equations (3-5) can be established to identify the Hill material parameters, while the first two also provide the Hosford parameters:

$$r_{0°} = \frac{\dot{\varepsilon}_2^p}{\dot{\varepsilon}_3^p} = \frac{H}{G} \quad (3)$$

$$r_{90°} = \frac{\dot{\varepsilon}_1^p}{\dot{\varepsilon}_3^p} = \frac{H}{F} \quad (4)$$

$$r_{45°} = \frac{\dot{\varepsilon}_{yy(\alpha=45°)}^p}{\dot{\varepsilon}_3^p} = \frac{2N - F - G}{2(F+G)} \quad (5)$$

The relations $H+G=2$ for Hill 1948 and $H+G=1$ for Hosford 1979 complete the system of equation. The Lankford coefficient and the initial yield stress appear in Table 1 for the DC06.

TABLE 1. Lankford coefficients, yield stress for DC06.

| $r_{0°}$	$r_{90°}$	$r_{45°}$	$\sigma_0\,(\varepsilon_0^P=0.2\%)$ [MPa]
1.98	2.56	1.67	142

The second identification method is mainly based on the plastic stresses measured by tensile, plane-strain and simple shear tests. The plastic work W_p at plastic strain of 0.2% is computed from the tensile test in RD. At equal W_p, a set of (σ_{xx}, σ_{yy}) is obtained from the other tests. The components of the plane-strain state are $\sigma_1 \neq \sigma_2 \neq 0$ and none of them is negligible. The stress resulting from the applied load is the only one that can be measured, i.e., σ_1 for plane-strain test at RD and σ_2 for plane-strain at 90° from RD (TD). To establish a relationship between the two components of this stress state, the flow rule with the fact that $\dot{\varepsilon}_2^p = 0$ for the

test in RD and $\dot{\varepsilon}_1^p = 0$ for the one in TD, is used. The simple shear test at 45° from the RD represents a pure shear state at small strains.

To fit the material parameters, the error function (6) is minimized:

$$\chi = \sum_{i=1,j} (1-\eta) \left[\frac{\sigma_{\Phi i} - \sigma_{\exp i}}{\sigma_{0\exp}} \right]^2 + \eta \left[r_{\Phi i} - r_{\exp i} \right]^2 \quad (6)$$

where the sub-index Φ means the values deduced from the respective yield criterion, *exp* means values deduced from experiments and *j* the number of tests. η is a weighting factor defining the weight of stress and strain measurements. In what follows η is set to 0 in order to focus the study in stress measurement.
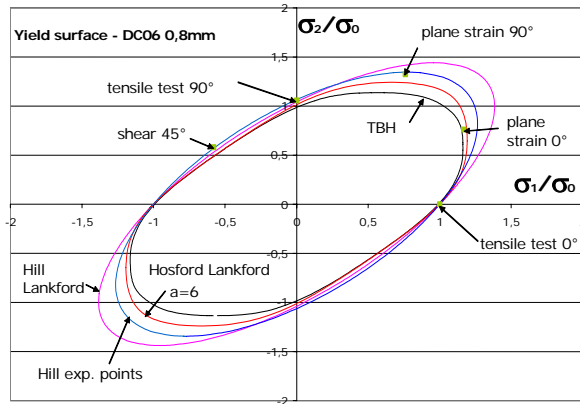
FIGURE 1. Scaled yield loci in principal stress directions and experimental points.

Figure 1 shows the Hill 1948 yield function fitted with Lankford coefficients (method 1) or with the 8 experimental points (method 2). These yield loci are compared with Taylor Bishop Hill (TBH) and Hosford surfaces. As underlined by Table 2 giving the parameters values, the Hosford yield locus identified by each described method is identical. One can observe that according to the experimental points, the quality of Hill identified by Lankford values is quite poor. The Hosford and TBH yield loci are close.

TABLE 2. Material parameters for DC06 steel

Material parameters	*H*	*F*	*G*	*N*	*a*
Hill 1948 Lankford	1.33	0.52	0.67	2.58	-
Hill 1948 exp. points	1.22	0.64	0.78	2.82	-
Hosford 1979 Lankford	0.66	0.26	0.34	-	6
Hosford 1979 exp. points	0.66	0.25	0.34	-	6

All the experimental points are plotted in Fig. 2, which shows sections of TBH and Hill exp. points yield loci at shear 0, 57 and 72 MPa. The pure shear case is 82.4 MPa in the test, when predicted values by TBH and Hill are respectively 76 and 83 MPa.
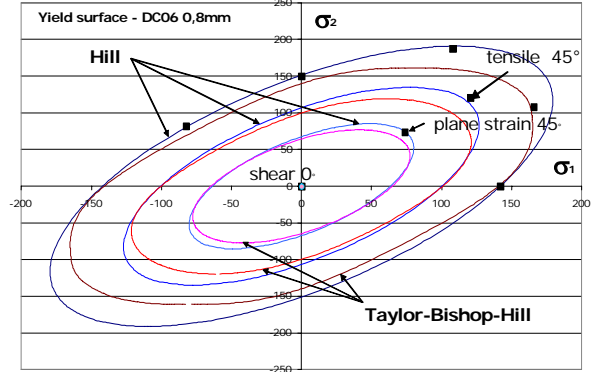
FIGURE 2. Sections in Hill and TBH yield loci at shear stress level 0, 57 and 72 MPa compared with associated experimental points.

These results show that mechanical tests reproducing other stress states than pure tension are required to obtain more accurate material parameters identification.

Hardening Model

The mechanical tests already described in previous section have been applied on the dual phase steel DP1000, 1.6 mm thick. The tests performed at 0°, 45° or 90° provide nearly superposed curves, while the Lankford coefficients (Table 3) also show a weak anisotropy.

TABLE 3. Lankford coefficients, yield stress for DP1000.

r_0	r_{90}	r_{45}	$\sigma_0(\varepsilon_0^P=0.2\%)$ [MPa]
0.86	0.88	0.996	697

In this case, identifying the Hill 1948 yield locus by method 1 or 2 provides identical results, summarized in Table 4.
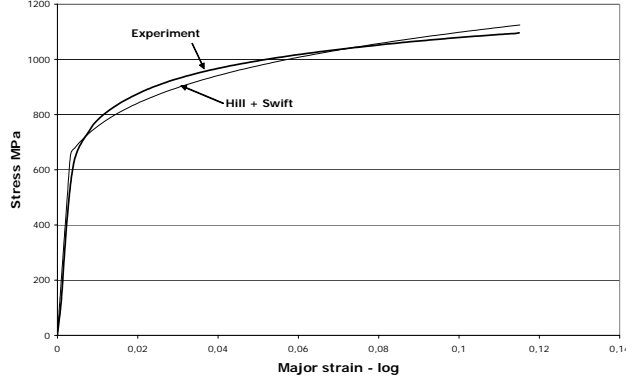
TABLE 4. Hill material parameters for DP1000.

H	*F*	*G*	*N*
0.925	1.051	1.076	3.182

First a simple isotropic model of Swift's law (equation (7)) is adjusted to the tensile test (Fig. 3):

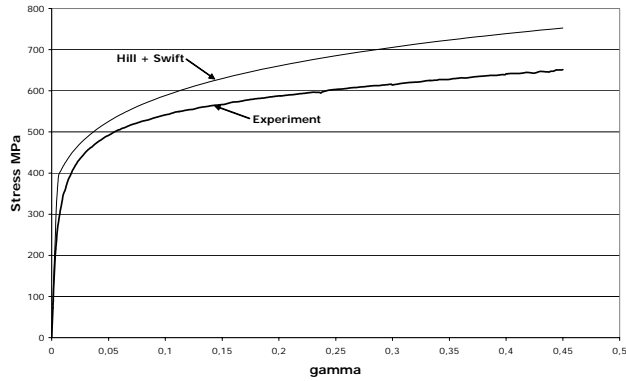$$\sigma_F = K\left(\varepsilon_0 + \overline{\varepsilon}^{\,p}\right)^n, \qquad (7)$$

with following material parameters K=1626 MPa, n=0.17 and ε_0 =0,00487.

**FIGURE 3.** Experimental tensile test in Rolling Direction and prediction of isotropic Swift hardening model.

However if this set of parameters is used to simulate the shear test, the model lacks accuracy as shown in Fig. 4. Note that *gamma* is the tangent of the shear angle.

FIGURE 4. Simple shear test simulation using an isotropic hardening law and experimental curve.

One could argue that, as the maximum strain in tensile test is 12% compared to 45% in shear, the isotropic hardening law should be fitted on the shear test. However, this strategy does not solve the discrepancy in the curve levels that then appears on the tensile test prediction curve. Another method could be to assume a texture updating that induces changes in the shape of the yield loci. The fact that all the tests performed at 0°, 45° or 90° provide nearly superposed curves is not compatible with such an anisotropic assumption. An alternative hypothesis is to assume that the N parameter accuracy is poor. However, in

order to reach a good agreement of the model for both tensile and shear tests, its modification is too large to keep a correct law for a nearly isotropic material. In fact, as checked by Baushinger shear tests shown in Fig. 5, this material shows kinematic hardening which already affects monotonic curves.
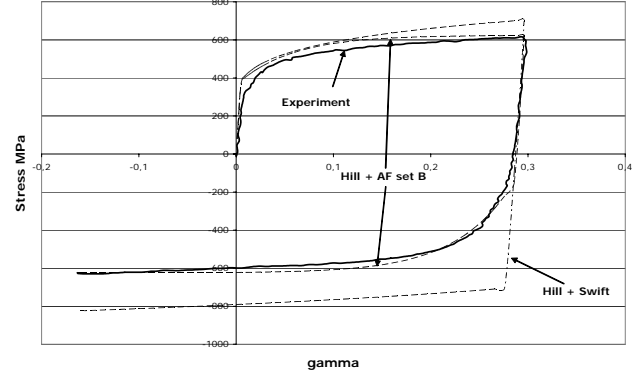
FIGURE 5. Shear Baushinger test and simulation by an isotropic hardening and a kinematic hardening (set B).

Reversed shear tests performed after 10, 20, 30 and 40% of pre-shear strain confirm that a simple kinematic hardening model of the Armstrong–Frederick (AF) type is sufficient, since no effect of the pre-shear level is observed. The evolution of the back-stress $\underline{X}$ is defined by equation (8):

$$\underline{\dot{X}} = C_X \cdot \left(X_{SAT} \cdot \underline{\dot{\varepsilon}}^P - \dot{\overline{\varepsilon}}^P \cdot \underline{X} \right) \qquad (8)$$

where C_X is the parameter describing the rate of kinematic hardening and X_{SAT} the saturation value.

The material parameters are fine-tuned up using an optimization method that is mainly based on Marquardt's algorithm [7] in order to fit the stress-strain experimental curves obtained from tensile or simple shear tests and the Baushinger experiment with 30% of pre-strain.

Two sets of parameters are compared set A, which models the tensile test more accurately, and set B, which is adjusted to have a better approach of the simple shear test. The initial value of the plastic stress in a tensile test is σ_0.

TABLE 5. Kinematic material parameter for DP1000.

Parameter Set	σ_0 (Mpa)	C_X	X_{SAT} (MPa)
A, adjusted on tensile test	697,34	56	197,3
B, adjusted on shear test	697,34	43,7	199

Figures 5, 6 and 7 compare the simulations using different sets of material parameters with experimental results. For the tensile test (Fig. 6), the best fit is obtained by the kinematic hardening using parameters set A.
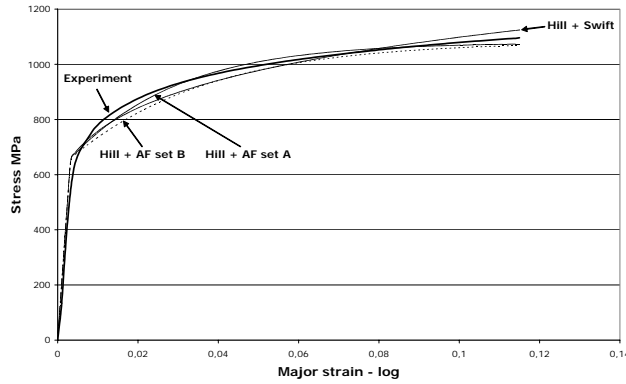
FIGURE 6. Tensile test simulated by isotropic hardening, kinematic hardening set A and B and experimental curve.

In the case of shear test (Fig. 7), the best prediction is given by the kinematic hardening. There is a slight difference between the curve obtained with set A and set B material parameters. The last one is closer to experimental values at smaller deformations. After 20% of strain, both results are coincident as the saturation parameter X_{SAT} is almost identical for both cases.
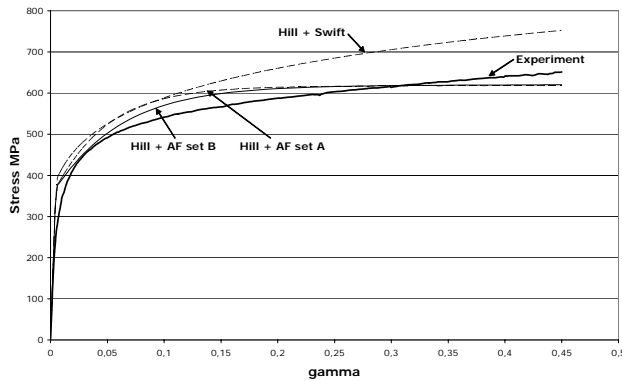
FIGURE 7. Shear test simulated by isotropic hardening, kinematic hardening set A and B and experimental curve.

As the Baushinger test is performed by two subsequent simple shear tests, the kinematic hardening model with set B gives the best fit. Fig. 5 compares this approach with the isotropic one. Isotropic hardening does not describe the Baushinger effect.

To conclude, this material presents a weak initial anisotropy and hardening behavior of kinematic type. Isotropic hardening must be avoided since it is not able to describe other stress states than the tensile one, even in monotonic loadings, as shown in Fig. 4.

APPLICATIONS

Single Point Incremental Forming

Process Description

The incremental sheet forming process has emerged in the past few years as a potential alternative to conventional sheet metal stamping processes. The process uses a smooth-ended tool under numerical control to create a local indentation in a clamped sheet. By dragging the point of contact around the sheet according to a programmed tool path, a wide variety of shapes may be formed without the need for specific tooling. Two versions of the process have been explored: with and without a supporting post on the reverse side of the workpiece. This section will only focus on the latter approach, called ´single point´ incremental forming (SPIF) presented in Fig. 8.
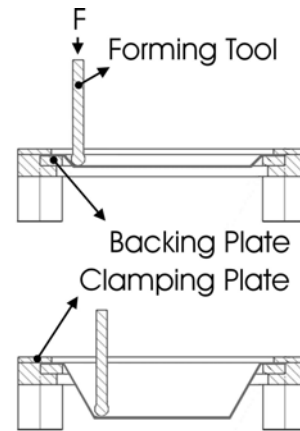

FIGURE 8. Single point incremental forming process.

The review paper [8] summarizes some fundamental research work carried out to investigate the deformation mechanism and material behavior. FEM simulations of this process are quite heavy as the tool path is very long and, if no remeshing module with numerous refinement and coarsening steps is used, a refined mesh is necessary everywhere as the tool induces very localized plastic strain.

Case Study

Figure 9 presents the Single Point Incremental Forming process of a cone of aluminum alloy AA 3003-O material. The dimensions of the initial sheet are 225x225x1.2mm. The cone wall angle is 50° and the cone depth 40mm. The steel tool has a diameter of 12.7mm and its vertical step size is 0.5mm. Tool forces were measured during the process [9] and the final shape was measured offline by laser scanning.

The flow stress curve of the material obtained by tensile tests is approximated by the Swift law $\sigma=180(\varepsilon+0.00109)^{0.21}$ (MPa). Two different yield criterion were used: Hill 1948 identified from the Lankford coefficients $r_0=0.68$, $r_{90}=0.66$ and $r_{45}=0.78$, and the isotropic von Mises law.
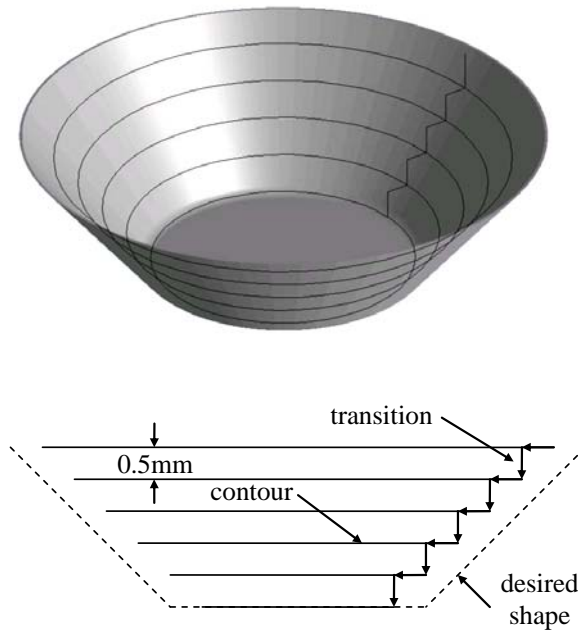

FIGURE 9. SPIF process of one 50° cone.

Geometrical Simulations Results

All the SPIF simulations commented hereafter are performed with the commercial FEM package Abaqus/Standard by the K.U.Leuven team. Brick elements with reduced number of integration points (element type C3D6 and C3D8R in the terminology of Abaqus) are utilized for the blank. The mesh consists of three layers of elements through the thickness. It covers either a 40° pie shape as presented in Fig. 10, a 90° pie or the full circular blank. The simulations

reported in this section only uses the above isotropic Swift hardening model.
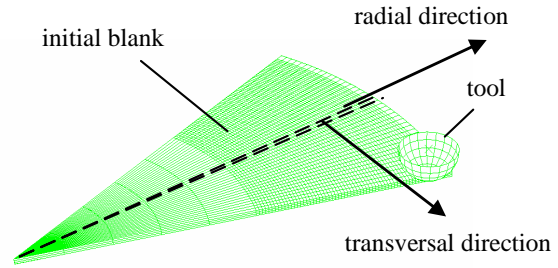
FIGURE 10. Mesh used to simulate Cone SPIF process.

The results from [10] and [11,12], confirmed by other research teams [13,14], show that concerning the exact shape prediction at the end of the process, the type of constitutive models is not a key factor. The discrepancy between the prediction from a 40° pie mesh and the experiment is shown in Fig. 11. FEM simulation is accurate in the wall region but predicts a cone bottom that is too deep compared to experimental results.
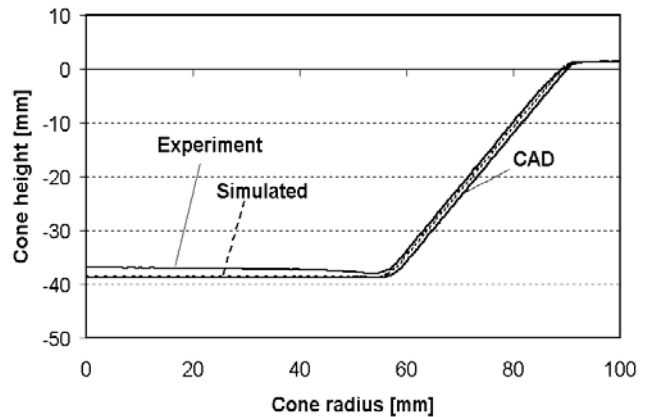

FIGURE 11. Top surface of the cross section of the formed cone.

However, for the same conical shape, it has been demonstrated that using a pie mesh of 90° or a full circular blank improves the prediction. The actual process is not symmetric and symmetry boundary conditions introduce additional stiffness that spoils the accuracy, see Fig. 12 [12].
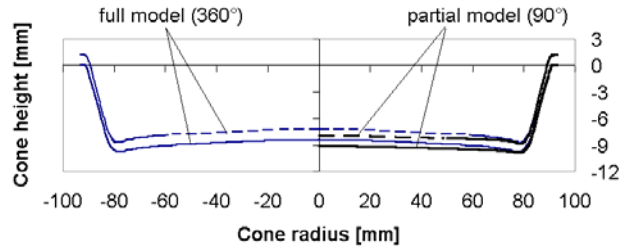
FIGURE 12. Comparison of resulting geometries obtained with partial and full model simulations using Abaqus (at an intermediate step).

In comparison with the effect of the model geometry, the effect of the constitutive model is smaller, as shown in Fig. 13.
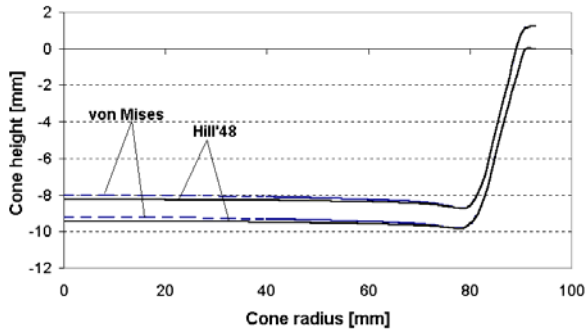

FIGURE 13. Comparison of resulting geometries with Von Mises or Hill 1948 constitutive laws.

Force Analysis

As shown in Fig. 14 [11], tool force measurements during the process allow another validation of the FEM simulations. When the mesh is sufficiently refined, the force level is not dependent on the dimensions of the pie.. Models of 40°, 90° pie or full 360° circular blank using Von Mises or Hill constitutive laws with isotropic hardening have provided nearly identical results: a prediction about 30% higher than the measurements

To understand this difference, the strain history of a material point has been analyzed during the process in a local coordinate system that co-rotates with the finite element. In Fig. 15, the strain history of an element localized at the origin of the local tangential axis defined in Fig. 10 has been drawn. The oscillations result from the fact that during each circular tool path 'arc' at one z level, strain only appears when the tool is near or on this element. It is clear that the absolute values of the axial (thickness direction), radial and tangential components increase stepwise during the process as shown in Fig. 15. However, it is noticed that the tangential strain is very

close to zero through the process, which confirms the plane strain assumption for theSPIF process.
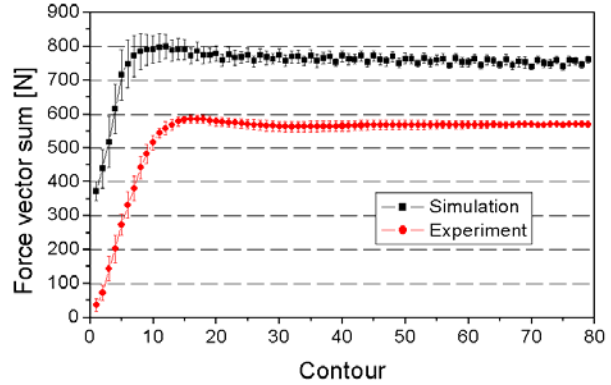

FIGURE 14. Force measurements during SPIF process and Abaqus predictions.
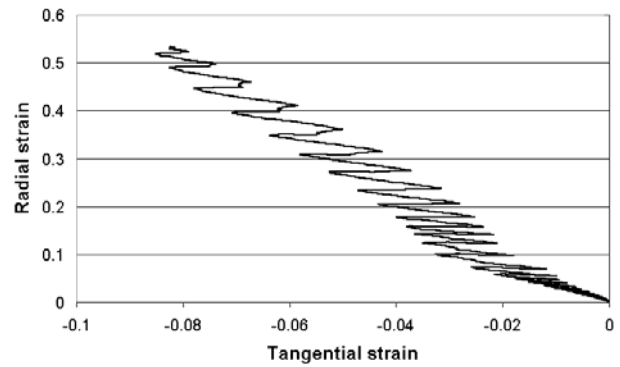
**FIGURE 15.** Plastic strain mode during SPIF process.

Knowing this strain history, the material behavior has been analyzed in more detail. First the yield locus shape computed by a TBH model has been drawn and compared to Hill, Von Mises and Hosford models in Fig. 16. Here axis 1 is the rolling direction and 2 the transversal direction in the sheet plane.
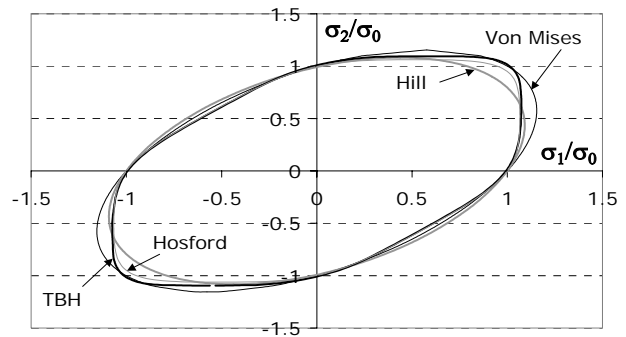
FIGURE 16. Initial scaled yield locus of AA3003-O.

In the plane strain regions of the surface in both rolling or transversal directions, differences between all the surfaces clearly appear. Although this fact may explain the small geometrical differences predicted by Hill and Von Mises models concerning the cone bottom geometry, further research is needed.

A second investigation concerns the hardening behavior model. Baushinger shear tests were used as in the identification method applied to the DP1000. The tests show a non-negligible kinematic hardening behavior as shown in (Fig. 17).
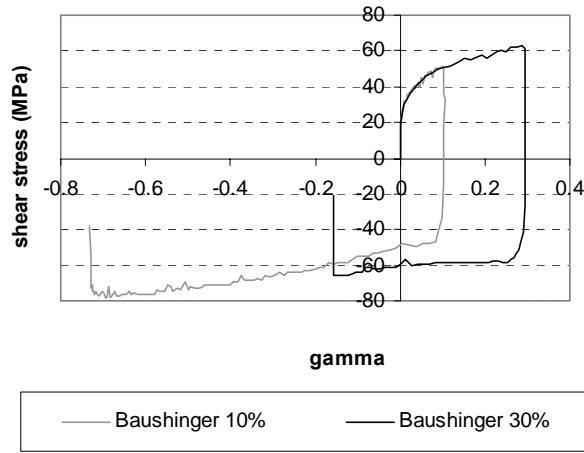
FIGURE 17. Experimental Baushinger tests with 10% and 30% of pre-shear.

Clearly the pre-shear performed in the first part of the Baushinger test has an effect on the shape of the curve during the second shear. A more complex model than Armstrong–Frederick could clearly be used.

However, taking into account the high computation time required by SPIF simulations, a first approach consists in identifying the best set of parameters using the Hill 1948 yield locus coupled with Swift isotropic hardening and Armstrong–Frederick (AF) kinematic hardening models.

Table 6 summarizes the set of parameters for the three models that have been used to simulate the strain history of Fig. 15 using only one finite element. This simulation as well as the identification by inverse modeling have been performed by the ULg team with their home-made FEM package Lagamine [15].

TABLE 6. Material set of parameters for AA 3003-O

|	Hill L + Swift	Hill L + Swift + AF	Hill A + Swift
F	1.2241	1.2241	1.2241
G	1.1933	1.1933	1.1933
H	0.8067	0.8067	0.8067
$L=M=N$	2.977	2.977	4.06
$K\ [MPa]$	183	183	183
ε_0	0.00057	0.00057	0.00057
n	0.229	0.229	0.229
C_X	0	3.137	0
X_{SAT}	-	11.06	-
m	1	0.381	1

The parameter m represents a balance between kinematic and isotropic hardening by modifying. equation (7) as follows:

$$\sigma_F = K\left(\varepsilon_0 + m\cdot\overline{\varepsilon}^{\,p}\right)^n. \qquad (9)$$

The evolution law of the back stress remains identical to equation (8). "Hill L" means the Hill 1948 model the parameters of which are computed using the Lankford coefficients. The "Hill A" model has the same parameters as "Hill L" except that the shear parameter L has been adjusted to fit the measurements of the monotonic simple shear test. Figs. 18, 19 and 20 respectively show the model predictions compared to monotonic tensile, simple shear and Baushinger tests in the RD. One can observe that the "Hill L + Swift" model only predicts the tensile test accurately. "Hill L + Swift + AF" predictions are closer to monotonic simple shear and Baushinger test results but do not match the experimental tensile curve well. "Hill A + Swift" seems to fit all the experimental results. However in the principal stress plane, where parameters F, G, H determine the yield locus shape, it is not so close to the yield surface computed by the TBH model. Another point is also that it does not reproduce the r_{45} value.

It is not a straightforward task to link those results, obtained using one finite element, to the force measured during the SPIF process. The accumulated plastic work during each tool path arc or "step" is plotted in Fig. 21. As the average displacement applied on the element during one arc is known, a force representative of this arc can be computed as the average plastic work divided by the average displacement, as shown in Fig. 22.
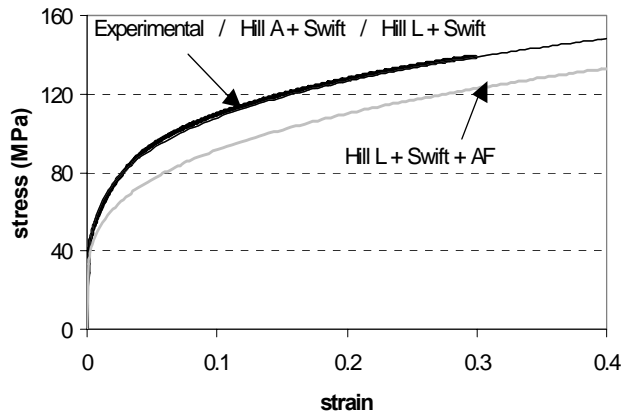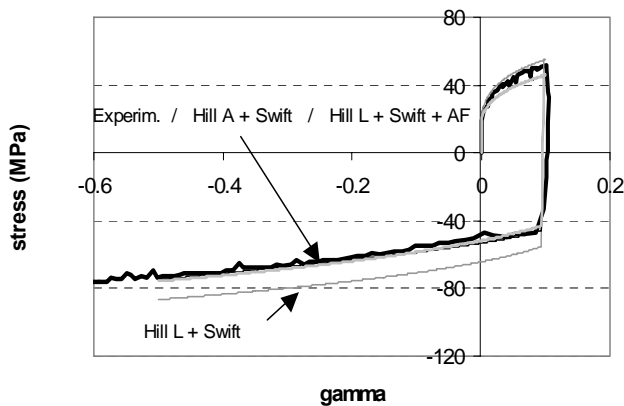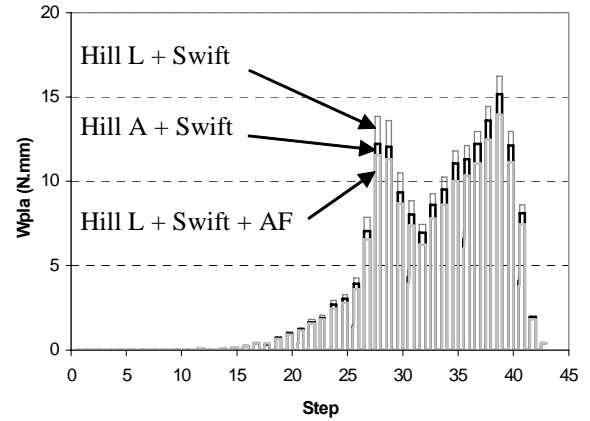
FIGURE 18. Experimental results and numerical predictions for a monotonic tensile test.
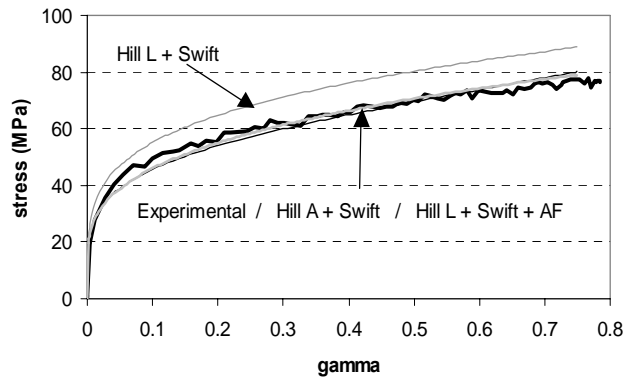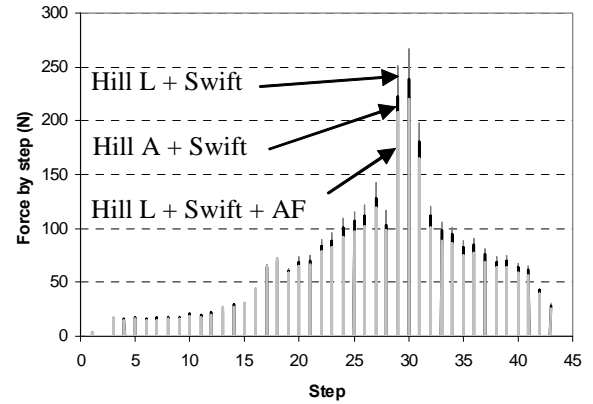

FIGURE 19. Experimental results and numerical predictions for a monotonic shear test.

FIGURE 20. Experimental results and numerical predictions for a Baushinger test with 10% of pre-shear.

FIGURE 21. Evolution of the accumulated plastic work during one arc.

FIGURE 22. Evolution of the representative tool force during each arc.

Table 7 gives values of this force for the 30th arc and clearly shows that the 30% of discrepancy observed between the Abaqus prediction with Hill + Swift and the experimental force measurements could decrease if either another yield locus shape or a mixed hardening model was used.

TABLE 7. Comparison of model Prediction

Model	Representative Arc Force (N)
Hill L + Swift	266.8
Hill L + Swift + AF	220.6
Hill A + Swift	238.0

In practice, both the shape of the yield locus and the hardening model should be improved to increase the accuracy of numerical force predictions during the SPIF process.

Cup Deep Drawing

In deep drawing, a classical test to check the effect of the yield locus shape and the hardening law is to measure the earing profile of a circular cup obtained from a circular blank using the deep drawing process.

All the details about experimental set up as well as mesh refinement, friction model and the material set of parameters can be found in [16] (presented in this NUMISHEET 2005 conference) and [17]. The current section is only focused on the choice of the yield locus and the hardening model.

The material is an interstitial free (IF) steel. The texture has been measured by the K.U.Leuven team and Teodosiu's isotropic and kinematic hardening model [3] was identified by Teodosiu's co-workers at University Paris 13 [16,17]. The interest of this quite complex hardening model is that it predicts the effect of strain path changes. For instance, in a Baushinger test as shown in Fig. 17, it can simulate the different stagnation in the hardening after the reverse loading according to the amount of applied pre-shear. In a cup deep drawing, the bending and unbending phenomena occuring at the die shoulder are far from a monotonic strain path and as observed in the following results, it requires a good hardening model to accurately predict the earing profile.

Three different yield loci have been applied to simulate the cup deep drawing and each one was either coupled with the isotropic Swift model (equation (7)) or with Teodosiu's model. Hill 1948 was identified from Lankford coefficients computed by the Taylor-Bishop-Hill yield locus provided by the texture. The second model is a micro-macro one, called Minty [18], that locally interpolates the stress-strain relation from yield locus points computed by a polycrystal Taylor model corresponding to the initial texture. The third model called Evol is similar to Minty but takes into account texture updating due to plastic strains. At each interpolation point and each time step, the set of 2000 orientations chosen to represent the texture is updated by a Taylor model. Details on Evol and Minty models as well as experimental validations of their predictions (earing profile or final texture) can be found in [18,19].

Figure 23 shows the yield loci computed by the Hill model and by Minty law, either based on the initial texture or on the final one, computed by Evol for one element in the middle of the vertical wall cup along the initial RD. The effect of texture updating seems low. However, it is well known that small changes in yield locus shape can induce significant

differences in plastic flow. Note that the Lankford coefficients predicted by initial texture are $r_{0°}=2.315$, $r_{45°}=1.742$ and $r_{90°}=2.325$, whereas the values related to the final texture are $r_{0°}=2.778$, $r_{45°}=1.834$ and $r_{90°}=1.550$.
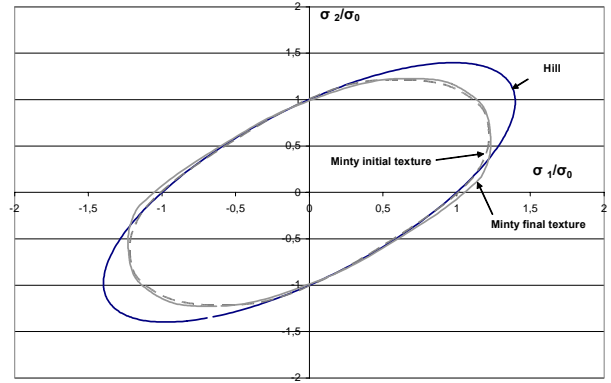

FIGURE 23. Yield locus shape computed by the 3 models.
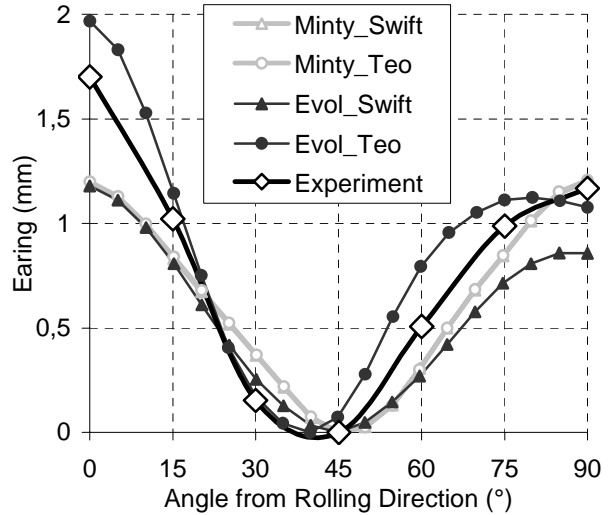

FIGURE 24. Comparison between earing measurements and numerical predictions.

Figure 24 presents the earing profile predicted by Minty and Evol coupled either with the Swift or Teodosiu hardening model. Hill results predict for both hardening models a minimum at 45° and a high amplitude of 3.3 mm, which modifies the Fig. 24 scale and prevents analysis of the details of the other law predictions, so it is not plotted. Minty law, which neglects texture evolution, predicts a minimum at 45° and no effect of the hardening model. Evol law shows a different earing when coupled with the Swift or Teodosiu hardening models. The isotropic case (Swift) predicts a minimum at 45° and a too low amplitude,

while the mixed hardening law of Teodosiu is closer to the experimental amplitude and predicts a shift of the minimum towards 40° in agreement with the experiment. However, an additional maximum not confirmed by the experiment appears in the Evol + Teodosiu case.

In this case, it seems that taking both texture updating and complex isotropic and kinematic hardening into account improves the accuracy of the final geometry computed by finite element models.

CONCLUSIONS

This paper underlines that the identification method of models is far from being trivial and without consequence for the accuracy of FEM model predictions. When working on the adjustment of the constitutive law parameters, one cannot decouple the yield locus shape from the hardening model, even if it would be easier for automatic parameter identification. Different choices of models are possible and the user must guide the research of material parameters knowing which models are available in his FEM code, the quality and the number of his experimental results and also his goal. Is it a first coarse analysis or does it require very accurate geometry or force predictions?

Two applications have been investigated. The predicted force computed during a SPIF process according to the assumption of isotropic or kinematic hardening model has been presented. In this case, a Hill model coupled with simple kinematic hardening improves the numerical prediction of forces. However a modified yield locus shape coupled with isotropic hardening provides also interesting results. Further simulations of the total process should validate which model better represents the actual material behavior.

For cup deep drawing, the FEM simulation results provided by the simple phenomenological Hill 1948 criterion are compared to the ones computed by more complex yield loci and hardening models. The earing prediction shows the interest of a micro-macro approach that takes both the texture updating and the Teodosiu's hardening model into account.

ACKNOWLEDGMENTS

REFERENCES

1. Flores, P., Moureaux, P., and Habraken, A.M., *Int. J. of Forming Processes* to appear (2005).
2. Armstrong, P.J., and Frederick, C.O., "A mathematical representation of the multiaxial Baushinger effect", Technical Report RD/B/N731, CEJB, 1966.
3. Bouvier, S., Teodosiu, C., Haddadi, H., and Tabacaru, V., *Journal de Physique IV* **105**, 215-222 (2003).
4. Van Houtte, P., 2002. ODFLAM Software, Part of the latest version of MTM-FHM Software System. Katholieke Universiteit Leuven.
5. Banabic B., Bunge, H.-J., Pöhlandt, K., and Tekkaya, A.E., *Formability of metallic materials* Springer 2000, pp. 139-140..
6. Hosford, W., *Materials Science & Engineering* A257, 1 – 8 (1998).
7. Marquardt, D.W., *J. Soc. Indust. Appl. Math.,*11, 431-440 (1963).
8. Jeswiet, J., Micari, F., Hirt, G., Bramley, A., Duflou, J., and Allwood, J., "Asymmetric Single Point Incremental Forming of Sheet Metal", *CIRP Annals 54/2* to appear (2005).
9. Duflou, J.R., Szekeres, A., and Vanherck, P., *Advanced Materials Research*, **6-8**, 441-448 (2005).
10. Henrard, C., Habraken, A.M., Szekeres, A., Duflou, J.R., He, S., Van Bael, A., and Van Houtte, P., *Advanced Materials Research,* **6-8**, 533-542 (2005).
11. He, S., Van Bael, A., Van Houtte, P, Szekeres, A., Duflou, J.R., Henrard, C., and Habraken, A.M., *Advanced Materials Research* **6-8**, 525-532 (2005).
12. He, S., Van Bael, A., Van Houtte, P., Tunckol, Y., Duflou, J., Henrard, C., Bouffioux, C., and Habraken, A.M., "Effect of FEM choices in the modelling of incremental forming of aluminium sheets", in *Proceedings of the 8th ESAFORM Conference on Material Forming,* edited by Banabic D., The publishing House of the Romanian Academy, 2005, pp. 711-714.
13. Fratini, L., Ambrogio, G., Di Lorenzo, R., Filice L., and Micari, F., *CIRP Annals*, **53/1**, pp. 207-210 (2004).
14. Iseki, H., *Journal of Materials Processing Technology* **111**, 150-154 (2001).
15 Habraken, A.M., and Cescotto, S., *Int. Jl. Numerical Methods in Engineering,* **30/8**, 1503 – 1525, (1990).
16. Duchêne, L., de Montleau, P., El Houdaigui, F., Bouvier, S., and Habraken, A.M., in *these proceedings*.
17. Li S., Hoferlin E., Van Bael A., Van Houtte P., and Teodosiu, C., *Int. J. Plast.* **19**, 647-674 (2003).
18. Habraken, A.M., and Duchêne, L., *Int. J. Plast.* **20**, 1525-1560 (2004).
19. Duchêne, L., Godinas, A., Cescotto, S., and Habraken, A.M., *J. of Materials Processing Technology* **125-126**, 110-118 (2002).